Synthesis and Characterization of WS_2 Nanotubes

Jun Chen,* Suo-Long Li, Feng Gao, and Zhan-Liang Tao

Institute of New Energy Materials Chemistry, Nankai University, Tianjin 300071, P.R. China

Received October 10, 2002. Revised Manuscript Received January 2, 2003

High-purity WS_2 nanotubes were synthesized on a relatively large scale by thermal decomposition of amorphous/nano $(NH_4)_2WS_4$ in a floating hydrogen and thiophene atmosphere at a heating temperature of 360−450 °C. Extensive investigations of WS_2 nanotubes by scanning electron microscopy, high-resolution transmission electron microscopy, X-ray diffraction, X-ray photoelectron microscopy, and Brunauer−Emmett−Teller measurements were reported. Our improved route yielded large quantities of open-ended WS_2 nanotubes with an average length of 5 μm, an outer diameter of 25−50 nm, an inner diameter of up to 20 nm, and an interlayer spacing of 0.62 nm. The present study is also of interest because it provides a clue to better understanding the *inside out* growth mechanism of WS_2 nanotubes, and this can be extended for the synthesis of other metal-sulfide nanostructural materials.

1. Introduction

Inorganic fullerene-like nanoparticles and nanotubes, first reported by Tenne and co-workers in 1992,[1] have generated intense scientific interest owing to their promising electronic and mechanical properties. Substantial progress has been achieved in the use of WS_2 nanotubes as scanning probe microscope tips,[2,3] fullerene-like WS_2 and MoS_2 nanoparticles as excellent lubricants,[4,5] MoS_2 and WS_2 nanoparticles or nanotubes as heterogeneous catalysts,[6−8] and MoS_2 nanotubes as electrochemical hydrogen storage and lithium intercalation materials.[9−12]

To date, various synthetic methods for the production of macroscopic amounts of multiwall MX_2 (M = Ti, Zr, Hf, Nb, Ta, Mo, W, or Re; X = S, Se, or Te) nanotubes have been described, and further progress is still underway. Syntheses of these materials include gas−solid reactions,[1,13−25] chemical transport,[26−29] electron-irradiation activation,[30−35] in-situ heating,[36−41] and solution route.[42−44] After the first preparation of WS_2 nested inorganic fullerenes and nanotubes, Tenne et al.[13−20] have extensively studied the preparation of WS_2

* Corresponding author. E-mail: chenabc@nankai.edu.cn.

(1) Tenne, R.; Margulis, L.; Genut, M.; Hodes, G. *Nature* **1992**, *360*, 444.
(2) Homyonfer, M.; Alperson, B.; Rosenberg, Y.; Sapir, L.; Cohen, S. R.; Hodes, G.; Tenne, R. *J. Am. Chem. Soc.* **1997**, *119*, 2693.
(3) Rothschild, R.; Cohen, S. R.; Tenne, R. *Appl. Phys. Lett.* **1999**, *75*, 4025.
(4) Rapport, L.; Bilik, Y.; Homyonfer, M.; Cohen, S. R.; Tenne, R. *Nature* **1997**, *387*, 791.
(5) Chhowalla, M.; Amaratunga, G. A. J. *Nature* **2000**, *407*, 164.
(6) Mdleni, M. M.; Hyeon, T.; Suslick, K. S. *J. Am. Chem. Soc.* **1998**, *120*, 6189.
(7) Alperson, B.; Homyonfer, M.; Tenne, R. *J. Electroanal. Chem.* **1999**, *473*, 186.
(8) Chen, J.; Li, S. L.; Xu, Q.; Tanaka, K. *Chem. Commun.* **2002**, 1722.
(9) Chen, J.; Kuriyama, N.; Yuan, H. T.; Takeshita, H. T.; Sakai, T. *J. Am. Chem. Soc.* **2001**, *123*, 11813.
(10) Chen, J.; Li, S. L.; Tao, Z. L.; Zhang, L. Z. *Int. J. Nanosci.* **2002**, *1*, 295.
(11) Dominko, R.; Arcon, D.; Mrzel, A.; Zorko, A.; Cevc, P.; Venturini, P.; Goborscek, M.; Remskar, M.; Mihailovic, D. *Adv. Mater.* **2002**, *14*, 1531.
(12) Zak, A.; Feldman, Y.; Lyakhovitskaya, V.; Leitus, G.; Popovitz-Biro, R.; Wachtel, E.; Cohen, H.; Reich, S.; Tenne, R. *J. Am. Chem. Soc.* **2002**, *124*, 4747.
(13) Margulis, L.; Salitra, G.; Tenne, R. *Nature* **1993**, *365*, 113.
(14) Hershfinkel, M.; Gheber, L. A.; Volterra, V.; Hutchison, J. L.; Margulis, L.; Tenne, R. *J. Am. Chem. Soc.* **1994**, *116*, 1914.
(15) Feldman, Y.; Wasserman, E.; Srolovitz, D. J.; Tenne, R. *Science* **1995**, *267*, 222.
(16) Tenne, R. *Adv. Mater.* **1995**, *7*, 965.
(17) Feldman, Y.; Frey, G. L.; Homyonfer, M.; Lyakhovitskaya, V.; Margulis, L.; Cohen, H.; Hodes, G.; Hutchison, J. L.; Tenne, R. *J. Am. Chem. Soc.* **1996**, *118*, 5362.
(18) Frey, G. L.; Elani, S.; Homyonfer, M.; Feldman, Y.; Tenne, R. *Phys. Rev. B* **1998**, *57*, 6666.
(19) Tenne, R.; Homyonfer, M.; Feldman, Y. *Chem. Mater.* **1998**, *11*, 3225.
(20) Rothschild, A.; Popovitz-Biro, R.; Lourie, O.; Tenne, R. *J. Phys. Chem. B* **2000**, *104*, 8976.
(21) Nath, M.; Govindaraj, A.; Rao, C. N. R. *Adv. Mater.* **2001**, *13*, 283.
(22) Nath, M.; Rao, C. N. R. *J. Am. Chem. Soc.* **2001**, *123*, 4841.
(23) Nath, M.; Rao, C. N. R. *Chem. Commun.* **2001**, 2236.
(24) Nath, M.; Rao, C. N. R. *Angew. Chem., Int. Ed.* **2002**, *41*, 3451.
(25) Brorson, M.; Hansen, T. W.; Jacobsen, C. J. H. *J. Am. Chem. Soc.* **2002**, *124*, 11582.
(26) Remskar, M.; Skraba, Z.; Cléton, F.; Sanjinés, R.; Lévy, F. *Appl. Phys. Lett.* **1996**, *69*, 351.
(27) Remskar, M.; Skraba, Z.; Regula, M.; Ballif, C.; Sanjinés, R.; Lévy, F. *Adv. Mater.* **1998**, *10*, 246.
(28) Remskar, M.; Skraba, Z.; Sanjinés, R.; Lévy, F. *Appl. Phys. Lett.* **1999**, *74*, 3633.
(29) Remskar, M.; Mrzel, A.; Skraba, Z.; Jesih, A.; Ceh, M.; Demsar, J.; Stadelmann, P.; Lévy, F.; Mihailovic, D. *Science* **2001**, *292*, 479.
(30) José-Yacamán, M.; López, H.; Santiago, P.; Galván, D. H.; Garzón, I. L.; Reyes, A. *Appl. Phys. Lett.* **1996**, *69*, 1065.
(31) Galván, D. H.; Rangel, R.; Alonso, G. *Fullerene Sci. Technol.* **1998**, *6*, 1025.
(32) Galván, D. H.; Kim, J. H.; Maple, M. B.; Avalos-Borja, M.; Adem, E. *Fullerene Sci. Technol.* **2000**, *8*, 143.
(33) Mackie, E. B.; Galván, D. H.; Adem, E.; Talapatra, S.; Yang, G. L.; Migone, A. D. *Adv. Mater.* **2000**, *12*, 495.
(34) Flores, E.; Tlahuice, A.; Adem, E.; Galván, D. H. *Fullerene Sci. Technol.* **2001**, *9*, 9.
(35) Galván, D. H.; Kim, J. H.; Maple, M. B.; Adem, E. *Fullerene Sci. Technol.* **2001**, *9*, 225.
(36) Zhu, Y. Q.; Hsu, W. K.; Grobert, N.; Chang, B. H.; Terrones, M.; Terrones, H.; Kroto, H. W.; Walton, D. R. M. *Chem. Mater.* **2000**, *12*, 1190.
(37) Hsu, W. K.; Zhu, Y. Q.; Boothroyd, C. B.; Kinloch, I.; Trasobares, S.; Terrones, H.; Grobert, N.; Terrones, M.; Escudero, R.; Chen, G. Z.; Colliex, C.; Windle, A. H.; Fray, D. J.; Kroto, H. W.; Walton, D. R. M. *Chem. Mater.* **2000**, *12*, 3541.

10.1021/cm020471f CCC: $25.00
Published on Web 02/01/2003

and MoS_2 nanotubes by heating tungsten or molybdenum oxides in $H_2S/H_2/N_2$ gas atmosphere at about 850 °C. Rao et al.[21−24] have successfully synthesized MX_2 nanotubes at high temperatures (800−1300 °C). Remskar et al.[26−29] reported the existence of MoS_2/WS_2 micro tubes, microribbons, and ropes formed by chemical-transport reactions at about 800 °C. Galvan et al.[30−35] described the production of MX_2 nanotubes by an activation method. Hsu and coauthors[36−41] employed an in situ heating technique to fabricate pure, doped, and coated MX_2 nanotubes. Other research groups used the solution low-temperature route to produce MoS_2 and WS_2 nanotubes.[42−44] For example, Li et al.[44] developed a direct pyrolysis method from artificial lamellar mesostructures for the synthesis of WS_2 nanotubes.

It can be seen that the above methods, in which either high temperature or complicated processes were adopted, may not be the best ones for obtaining a high-rate production of WS_2 nanotubes. On the other hand, because the catalytic and physical properties of nanotubes strongly depend on their size and shape, it is thus important to devise methods that allow significant control over the morphological attributes. From a viewpoint of applications, the emphasis of WS_2 nanotube growth will be on the synthesis of high-purity, high-yield, and low-cost product.

In this paper, we report the synthesis and characterization of open-ended WS_2 nanotubes that are obtained using a gas−solid reaction of amorphous/nano $(NH_4)_2WS_4$ in a floating H_2 and thiophene atmosphere at around 360−450 °C. The present work allows lower growth temperature and thus easier/safer control over the reaction process, and produces WS_2 nanotubes at high rate, high purity, and low cost.

2. Experimental Section

2.1. Three Steps to Prepare WS_2 Nanotubes. Our production for yielding WS_2 nanotubes is schematically shown in Figure 1. As can be seen, the process consists of three steps: (1) a procedure similar to that previously reported[45] was used to prepare needlelike tetrathiotungstate $(NH_4)_2WS_4$ from ammonium tungstate hydrate $(NH_4)_6W_{12}O_{39}\cdot 12H_2O$ (Aldrich, 99.9%); (2) ball milling of $(NH_4)_2WS_4$ in H_2 atmosphere (0.2 MPa with a Fuji Auto mixer[46] at 800 rpm for 1 h); and (3) sintering of the as-ball-milled sample in floating hydrogen and thiophene (C_4H_4S).

2.2. Heating Apparatus. The reaction to achieve WS_2 nanotubes was carried out in a conventional furnace with a horizontal alumina tube (Figure 2). Thiophene, which was used as a catalyst source, was vaporized and floated by pure hydrogen to produce a stream of mixing gas that was controlled by a mass-flow control system and flowed into the reactor at a rate of 60−150 mL/min. To avoid agglomeration at the heating reaction, $(NH_4)_2WS_4$ particles were carefully dispersed on the entire reactor substrate, resulting in complete exposure of the particle surface to the reacting gas. The reaction temperature was maintained at 360−450 °C with a K-type thermocouple. Synthesis times were adjusted with a maximum 30 min. The off-gases were introduced first to a dimethylformamide (DMF) solvent and then to a $ZnSO_4$ solution before they were vented into the atmosphere. After cooling to room temperature, the reaction products were collected on a quartz substrate for various analyses.

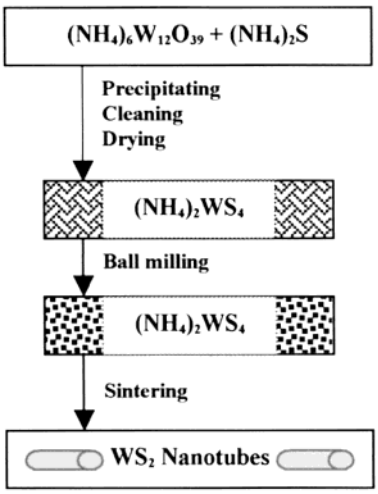

Figure 1. Reaction scheme used to synthesize WS_2 nanotubes.

2.3. Instrumental Analyses. Complementary information on the reaction mechanism was obtained by using a combination of the following techniques: scanning electron microscopy (SEM) equipped with energy-dispersive X-ray spectroscopy (EDXS), transmission electron microscopy (TEM) and high-resolution TEM (HRTEM), X-ray powder diffraction (XRD), X-ray photoelectron spectroscopy (XPS), and Brunauer−Emmett−Teller (BET) adsorption−desorption measurements.

Specimens for SEM were fixed to a piece of copper tape, which was attached to a SEM stub and then sputtered with a 2-nm layer of gold. Images were taken with a JEOL JSM-5600 scanning electron microscope working at an accelerating voltage of 20 kV. EDXS was performed in the microscope with use of a Kevex Super 8000 detector. Selected WS_2 nanotubes were clamped between two copper grids for TEM analysis, which was carried out in a Philips Tacnai F20 microscope operating at an accelerating voltage of 200 kV. XRD analysis was by a Rigaku INT-2000 X-ray generator. The X-ray intensity was measured over a diffraction 2-theta angle from 5 to 85° with a velocity of 0.02°/step and 2°/min. The surface of the reacted and unreacted samples was examined with the XPS (ESCA-3400, Shimadzu Electron) using a monochromatic Mg Kα radiation (1253.6 eV). The measured surface composition was an average over 0.20 cm^2 areas and 20−30 Å depths. The binding energy values were referenced to the carbon C 1*s* core peak at 284.7 eV. The specific surface areas and pore sizes were determined by BET at a bath temperature of 77.4 K using a nitrogen gas adsorption/desorption method (Shimadzu-Micromeritics ASAP 2010 Instrument). Prior to the desorption measurement each sample was degassed by heating at 150 °C and pumping for 5 h, and then the pressure was about 5×10^{-7} Torr.

3. Results and Discussion

3.1. Ball Milling Step. The specific surface areas (SSA) of the un-milled $(NH_4)_2WS_4$ were 1.2 m^2/g, but

(38) Zhu, Y. Q.; Hsu, W. K.; Terrones, H.; Grobert, N.; Chang, B. H.; Terrones, M.; Wei, B. Q.; Kroto, H. W.; Walton, D. R. M.; Boothroyd, C. B.; Kinloch, I.; Chen, G. Z.; Windle, A. H.; Fray, D. J. *J. Mater. Chem.* **2001**, *10*, 2570.
(39) Zhu, Y. Q.; Hsu, W. K.; Terrones, M.; Firth, S.; Grobert, N.; Clark, R. J. H.; Kroto, H. W.; Walton, D. R. M. *Chem. Commun.* **2001**, 121.
(40) Hsu, W. K.; Zhu, Y. Q.; Yan, N.; Firth, S.; Clark, J. H.; Kroto, H. W.; Walton, D. R. M. *Adv. Func. Mater.* **2001**, *11*, 69.
(41) Whitby, R. L. D.; Hsu, W. K.; Fearon, P. K.; Billingham, N. C.; Maurin, I.; Kroto, H. W.; Walton, D. R. M.; Boothroyd, C. B.; Firth, S.; Clark, R. J. H.; Collison, D. *Chem. Mater.* **2002**, *14*, 2209.
(42) Zelenski, C. M.; Dorhout, P. K. *J. Am. Chem. Soc.* **1998**, *120*, 734.
(43) Liao, H. W.; Wang, Y. F.; Zhang, S. Y.; Qian, Y. T. *Chem. Mater.* **2001**, *13*, 6.
(44) Li, Y. D.; Li, X. L.; He, R. L.; Zhu, J.; Deng, Z. X. *J. Am. Chem. Soc.* **2002**, *124*, 1411.
(45) Pan, W. H.; Leonowicz, M. E.; Stiefel, E. I. *Inorg. Chem.* **1983**, *22*, 672.
(46) Chen, J.; Kuriyama, N.; Xu, Q.; Takeshita, H. T.; Sakai, T. *J. Phys. Chem. B* **2001**, *105*, 11214.

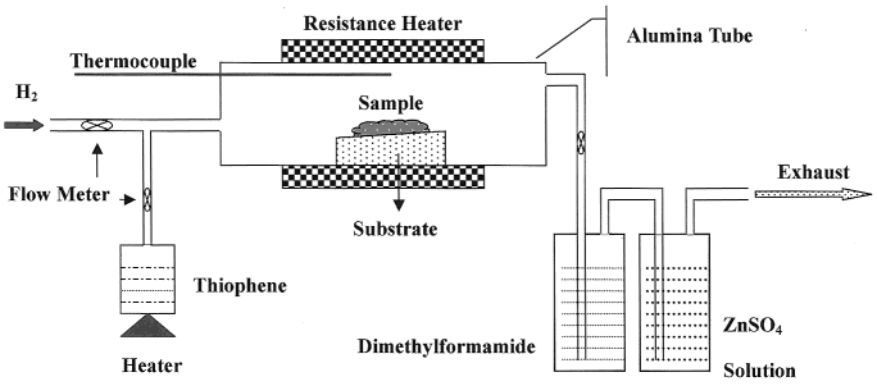

Figure 2. Schematic diagram of the heating apparatus used for the high-rate and high-quality synthesis of WS_2 nanotubes.

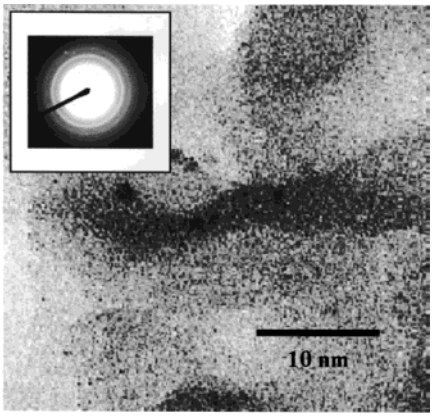

Figure 3. TEM image for amorphous/nano $(NH_4)_2WS_4$ particles after ball-milling process. Inset is the electron diffraction pattern.

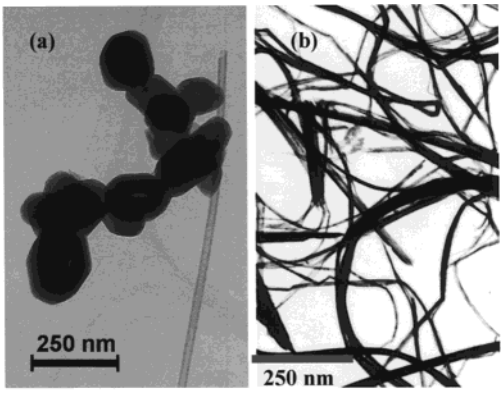

Figure 4. TEM images of the products synthesized with thiophene addition of (a) 0 vol % and (b) 5.0 vol % at 400 °C, 120 mL/min flow rate, and an annealing time of 30 min.

after ball milling for 1 h, the SSA increased to 11.5 m^2/g. Apparently, there is a characteristic increase in the SSA of this sample after ball milling. The XRD analysis shows that some peaks in the XRD pattern of the ball milled $(NH_4)_2WS_4$, in comparison with that of the un-milled sample, disappeared and the remaining peaks were relatively broader (Figure 9A, vide infra). These results indicate that the ball milling procedure offers the transformation of polycrystalline $(NH_4)_2WS_4$ to amorphous/nano particles, as confirmed by TEM investigation (Figure 3). The electron diffraction pattern exhibits amorphous haloes (inset of Figure 3), being consistent with the XRD analysis. Therefore, a prominent decrease in the grain size of $(NH_4)_2WS_4$ with defects was obtainable from the ball milling, and this led to an obvious increase in the SSA. Furthermore, XPS analysis shows that the binding energy of W $4f_{7/2}$ in the ball-milled $(NH_4)_2WS_4$ is 35.1 eV, which is in good agreement with that in the initial $(NH_4)_2WS_4$ (35.2 eV), illustrating that there is no valence change of W^{6+} during the ball-milling process.

It is worth noting that the ball-milling technique we use to provide amorphous/nano $(NH_4)_2WS_4$ particles plays an important role in obtaining nanotubes at low temperature due to the greatly enhanced reaction kinetics. As an example, heating the un-milled $(NH_4)_2WS_4$ in hydrogen and thiophene up to 600 °C did not yield the WS_2 nanotubes. However, using ball-milling treatment in a hydrogen atmosphere to "activate" the solid precursor could induce the growth of pure WS_2 nanotubes at a relatively low sintering temperature of about 360 °C.

3.2. Synthesis Conditions. In the synthesis of WS_2 nanotubes, different conditions of heating the amorphous $(NH_4)_2WS_4$ particles were investigated in detail in an attempt to understand how the WS_2 nanotubes grew and whether there were controls of the morphology of the tubes prepared. Variations in the conditions included changing the thiophene (catalyst) concentrations, the heating temperature, the flow rate, and the annealing time. In all these experiments, only one parameter was changed at a time.

Thiophene Addition. In the case of the thiophene addition, the liquid precursor was vaporized and co-floated with hydrogen gas, resulting in a vapor-phase catalyst. Notable differences could be observed in the absence and in the presence of the thiophene under the same conditions (400 °C, 120 mL/min, and an annealing time of 30 min). The products obtained by floating H_2 with thiophene were better crystallized than those acquired without thiophene (Figure 4). In Figure 4a without any addition of thiophene, WS_2 nanotubes were indeed formed, but nanoclusters coexisted. The addition of 2 vol % thiophene was found to be effective in increasing the quality of WS_2 nanotubes. With loading amounts of thiophene up to 5 vol %, WS_2 nanotubes were easily synthesized with a high yield and high purity (Figure 4b). This behavior can be further proven from the relation between the various amounts of thiophene and the pore size distribution of WS_2 nanotubes (Figure 5). The changing amounts of thiophene had no significant effect on the pore size range with radius between 1 and 500 Å. However, they showed a great influence on the pore size distribution: an increase

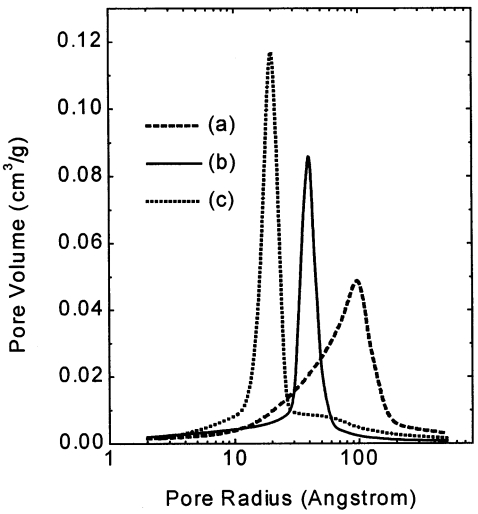

Figure 5. Effect of different thiophene amounts on the pore radius distribution of WS_2 nanotubes annealed at 400 °C and 120 mL/min for 30 min: (a) 0 vol %, (b) 2.0 vol %, and (c) 5.0 vol %.

of the loading amounts of thiophene catalyst up to 5 vol % caused a more narrow distribution of the pore radius around 20 Å, indicating the formation of WS_2 nanotubes with a smaller pore size and a more homogeneous pore distribution. Further increase of the loading amounts of thiophene higher than 5 vol % was found to show little difference. It should be noted that in any addition of thiophene, a gas chromatograph analysis detected no content-decrease of thiophene in the emerging gas mixture from the alumina tube, indicating that thiophene acts only as a growth-promoting catalyst.

Floating Gas Rate. The main process of the present synthesis of WS_2 nanotubes consists of the hydrogen reduction of $(NH_4)_2WS_4$. Thus, H_2 plays the role of the reducer and it is found to be indispensable for the growth of WS_2 nanotubes. To know the precise effect of the total flow rate on the growth and morphology of WS_2 nanotubes, only the floating gas rate was altered. When the flow rate was either lower than 75 mL/min or higher than 125 mL/min, nanotubes and nanoparticles were produced, whereas when the flow was between these two rates, only nanotubes were observed (Figure 6). In these three situations, defects were always observed in the surface, possibly reflecting the fact that the tube growth occurs from the *inside out*.

Heating Temperature. Because the folding of the WS_2 layers requires thermal energy, a detailed study of the heating temperature was undertaken to investigate the growth of WS_2 nanotubes. It was reported that annealing $(NH_4)_2WS_4$ at elevated temperatures (1200−1300 °C) yielded changes in crystallinity of WS_2 nanotubes.[19] In comparison, an excellent yield of WS_2 nanotubes/nanofibers was acquired by the direct heating of amorphous/nano $(NH_4)_2WS_4$ at a relatively lower temperature of 360−650 °C, using the hydrogen floated thiophene gas. Depending on the heating temperature, two kinds of morphologies had been observed: nanotubes (20−30 nm diam.) at 360−450 °C and nanofibers (15−30 nm diam.) at 470−650 °C, as shown in Figure 7. The WS_2 nanotubes or nanofibers appear to exhibit an almost cylindrical cross section, indicating that both the instant growth of WS_2 nanotubes in the first place and their

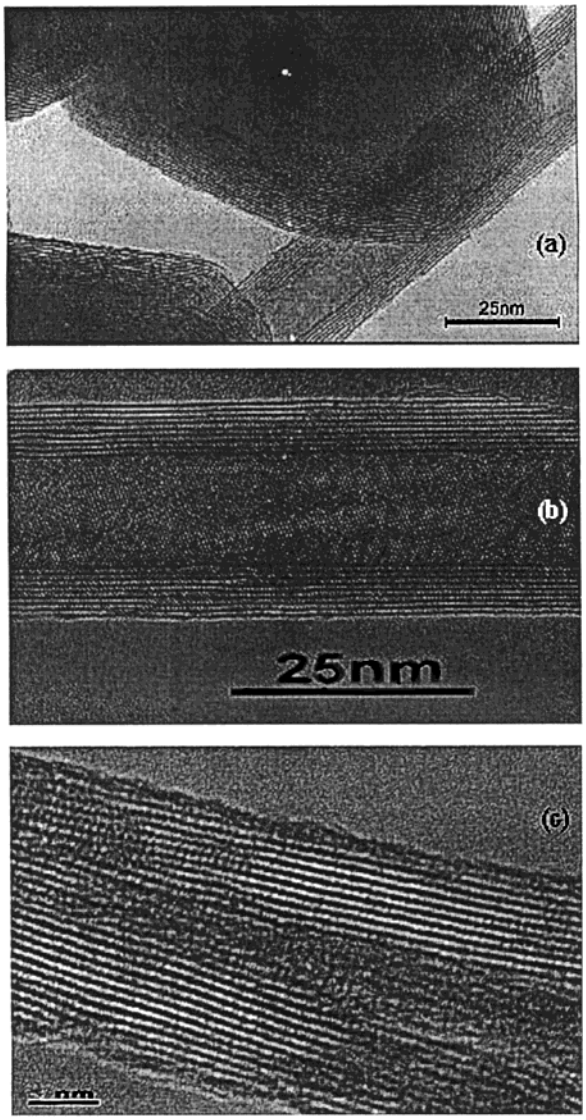

Figure 6. HRTEM images of the products obtained at various floating rates (FR): (a) FR < 75 mL/min; (b) 75 mL/min ≤ FR ≤ 125 mL/min; and (c) FR > 125 mL/min.

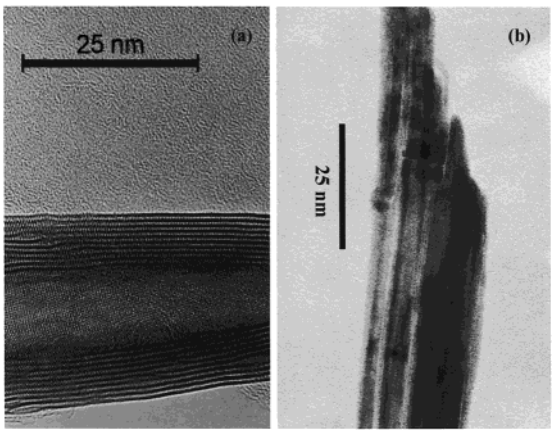

Figure 7. TEM images of the products obtained at (a) 360−450 °C (nanotubes) and (b) 470−650 °C (nanofibers).

subsequent growth have been affected by controlling the heating temperature. The morphology difference is because the energy input at high-temperature synthesis is too fast to form tubular structures. To further confirm this, low-temperature synthesis at 360 °C with short

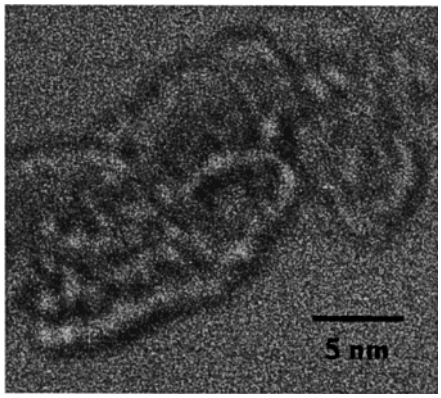

Figure 8. HRTEM image for a single-wall WS_2 nanotube.

Table 1. Specific Surface Areas (SSA) and Average Pore Radius (APR) of the Unmilled (UM) and Milled (M) $(NH_4)_2WS_4$, and WS_2 Nanotubes Obtained after Different Heating Times (H-5, 10, 30 min)

sample	SSA (m^2/g)	APR (Å)
$(NH_4)_2WS_4$ (UM)	1.2	99.8
$(NH_4)_2WS_4$ (M)	11.5	78.5
WS_2 (H-5 min)	7.8	52.3
WS_2 (H-10 min)	6.5	36.7
WS_2 (H-30 min)	5.2	20.6

reaction time (about 2 min) was applied. Figure 8 shows the embryo of a single wall WS_2 nanotube. At temperatures lower than 300 °C, the uniaxial growth is not induced. Therefore, the temperature is one key factor for synthesizing WS_2 nanotubes.

Growth Time. Another interesting observation about the phase formation of WS_2 nanotubes was also made with changing the growth time. Figure 9A gives the XRD patterns of WS_2 nanotubes synthesized at various stages of the annealing process. The XRD pattern of the sample without annealing coincides with that of $(NH_4)_2WS_4$ (ICDD-JCPDS Card 16-213), except the peaks broadening. After 5 min of annealing, a strong peak was observed at $2\theta = \sim 14°$, and this signals the growth of WS_2 phase (ICDD-JCPDS Card 8-237). After 10 min of annealing at the same conditions, we can clearly see the further growth of WS_2 phase. The fully converted sample is observed after annealing for 30 min. The diffraction peaks were relatively broadened, indicating that the final phase had fine grain size. The XRD patterns of the nanotubes gave hexagonal unit cell dimensions, suggesting that the WS_2 nanotubes are directly acquired by heating $(NH_4)_2WS_4$ nanoparticles in a flux of H_2/thiophene. The HRTEM images of the samples after different annealing time are shown in Figure 9B, which further confirms the formation of WS_2 nanotubes. The specific surface areas and average pore radius of the WS_2 nanotubes, obtained from the BET nitrogen adsorption/desorption method, are summarized in Table 1, from which it can be seen that both specific surface areas and average pore radius decreased. Therefore, on the basis of the above XRD, HRTEM, and BET analyses, we could deduce that the phase transformation of amorphous $(NH_4)_2WS_4$ to WS_2 nanotubes occurred.

Comprehensive Consideration. The principle for the present synthesis of WS_2 nanotubes is based on a catalytic gas−solid reaction, where large quantities (~5 g) of $(NH_4)_2WS_4$ particles were heated to a fixed temperature under the flow of a forming gas of H_2 and thiophene. The ball milling of $(NH_4)_2WS_4$ produced a nanocomposite phase, which greatly improved the kinetics for its transformation to WS_2 tube. Thiophene in a vaporized state strongly catalyzed the transformation of $(NH_4)_2WS_4$ to WS_2 at a low temperature. The formation of WS_2 nanotubes from $(NH_4)_2WS_4$ is a redox reaction, which can be described as follows:

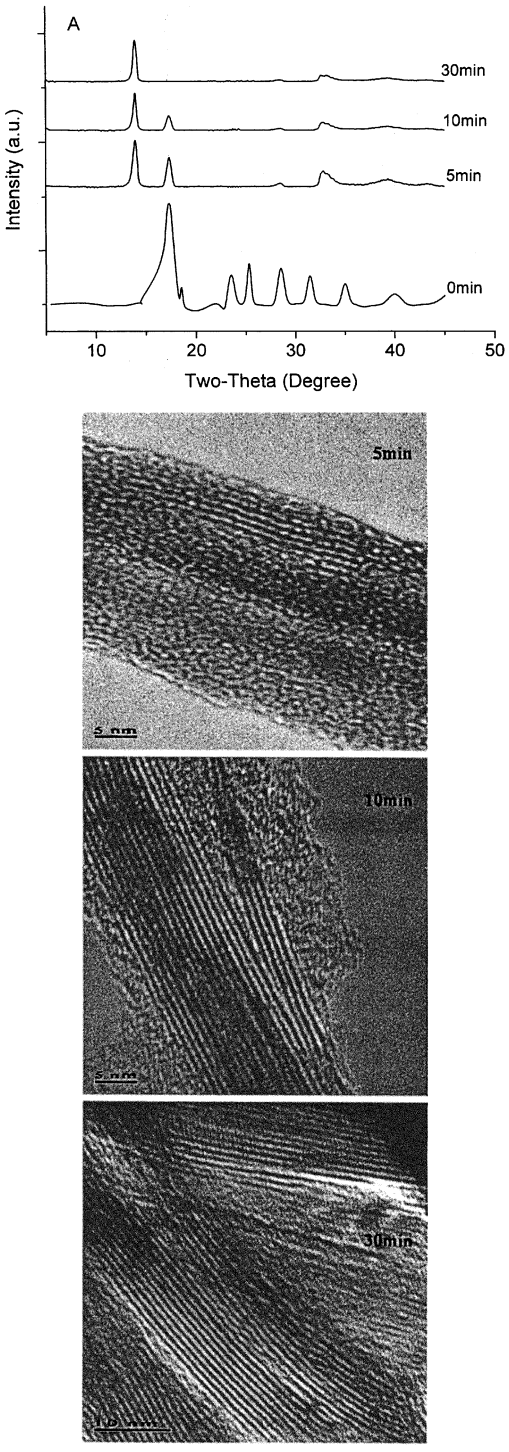

Figure 9. Transformation of amorphous/nano $(NH_4)_2WS_4$ particles to WS_2 nanotubes followed by (A) XRD taken on ball-milled $(NH_4)_2WS_4$ after heating for various times (0, 5, 10, and 30 min), and (B) related HRTEM images. Annealing conditions: 400 °C with hydrogen floated thiophene (volume ratio of 95:5) and gas flow of 120 mL/min.

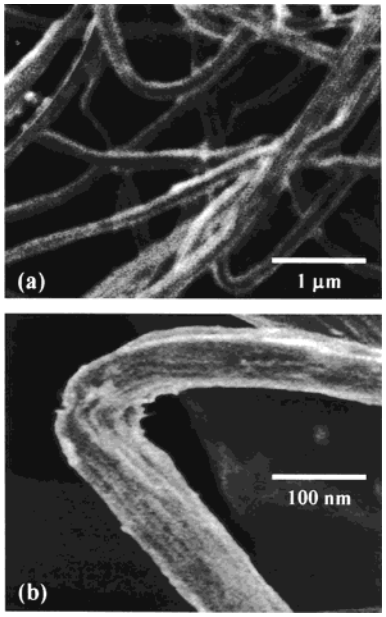

Figure 10. SEM images of the as-synthesized WS_2 nanotubes: (a) low-magnification image showing the nano-bundles with typical length of μm; (b) high-magnification image presenting the well-aligned nano-threads.

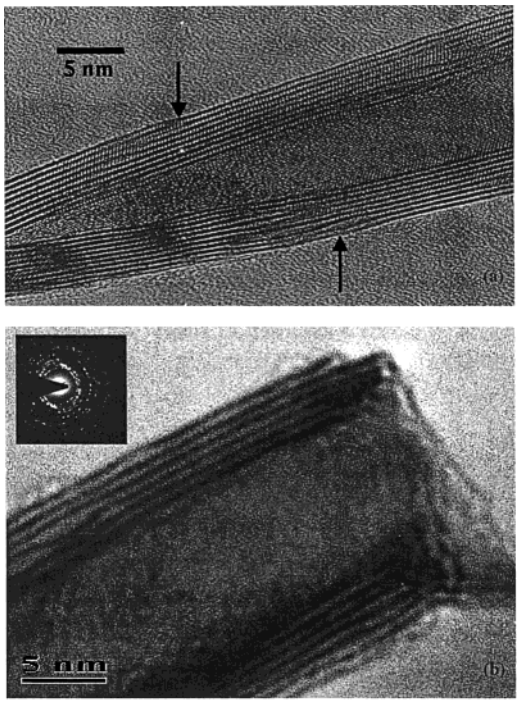

Figure 11. HRTEM image of (a) a horn-like WS_2 nanotube and (b) a typical edge of WS_2 nanotube, prepared by the annealing of $(NH_4)_2WS_4$ nanoparticles at 400 °C in a stream (120 mL/min) of H_2/thiophene (volume ratio of 95:5). Arrows mark the fork and termination defects.

$$(NH_4)_2WS_4 + H_2 \xrightarrow[\sim 400\ ^\circ C]{\text{Thiophene}} WS_2 + 2H_2S + 2NH_3 \quad (1)$$

At the same time, other synthesis parameters such as the heating temperature, the total flow rate, and the annealing time were also found to be important factors that are effective in changing the yield and the quality of WS_2 nanotubes. Consequently, to have a high-yield and high-purity phase of WS_2 nanotubes, the optimized conditions were determined to be a gas flow rate of 120 mL/min (volume ratio of H_2/thiophene 95:5), a heating temperature of 400 °C, and a total annealing time of 30 min.

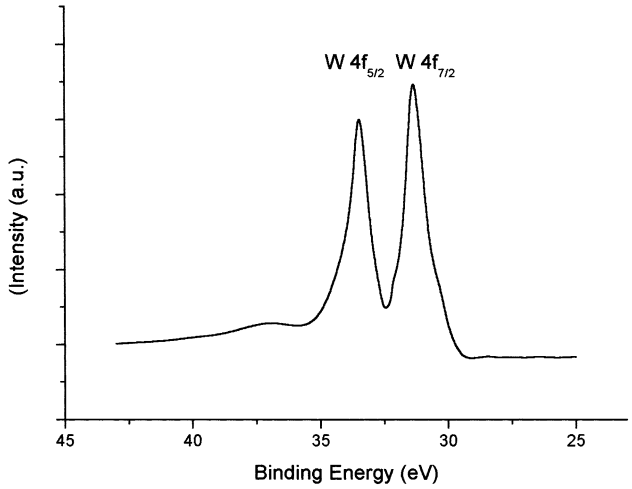

Figure 12. XPS of W 4f spectra of WS_2 nanotubes after complete reaction (after 30 min heating).

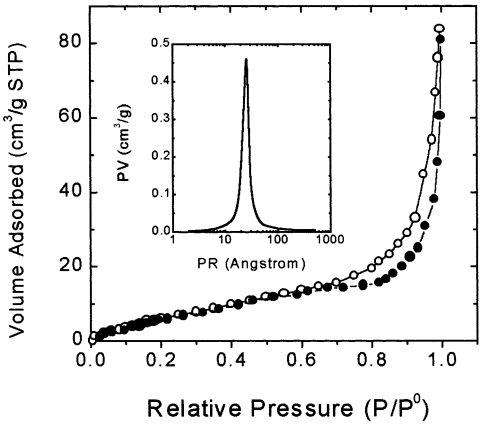

Figure 13. Nitrogen adsorption (line with solid circles) − desorption (line with open circles) isotherm, and pore-size distribution (inset) of WS_2 nanotubes.

Hereafter, we focused on the structural characterization of high-purity WS_2 nanotubes synthesized with the above optimized experimental conditions.

Figure 10 shows SEM images of the as-prepared products. From Figure 10a, a low-magnification image, we can see that the sample is in the presence of nanotubes with typical lengths of 100 nm. Figure 10b, of higher magnification, reveals that the nanotube is made of many well-aligned threads. EDXS spectra collected from the surface of the products demonstrate the presence of W and S, and the atomic ratio of W to S is 1:2. Figure 11 shows HRTEM images of a horn-shaped WS_2 nanotube and a typical open-ended edge of a nanotube. In both nanotubes, an interlayer spacing of ~0.62 nm is observed, which corresponds to the (002) plane of 2H−WS_2. The inset in Figure 11b shows the electron diffraction pattern, exhibiting a hexagonal arrangement of the tube layers. It is noteworthy that many defects consisting of fork and termination were found in the outside fringes of the tube (marked by arrows in Figure 11a), illustrating that defects are one of the important factors for the growing of multiwall nanotubes. This result suggests that any calculation of the structures and energetics in WS_2 nanotubes must

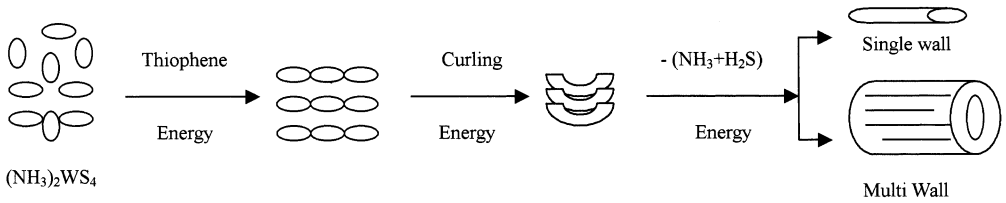

Figure 14. Schematic illustration of an *inside out* mechanism for fabricating WS_2 nanotubes.

consider the defects.[47,48] Figure 12 shows the W 4f spectrum of the nanotubes produced. The chemical valence of tungsten in the nanotubes contains only W^{4+}, because a binding energy of 31.4 eV was detected, being assigned to W $4f_{7/2}$ in WS_2.[49] On the other hand, the binding energy of S 2p (~162.0 eV) in the final synthesized sample is indeed S^{2-} form, as occurred in eq 1. This fact also shows that the stoichiometry of the final nanotube is WS_2, consistent with the EDXS result. Figure 13 shows the nitrogen adsorption−desorption isotherm of the WS_2 nanotubes. The adsorption−desorption cycle clearly shows the presence of a hysteresis loop at $p/p^0 > 0.7$, attributing to the capillary condensation associated with large pore channels.[50] The specific surface areas reach 5.2 m^2/g with a pore radius distribution at 20.5 Å.

3.3. *Inside Out* Growth Mechanism. The growth mechanism of MS_2 (M = Mo, W) nanotubes synthesized from MO_3 has been studied in some detail before.[51] It is believed that the nanotubes grow from MO_{3-x} nanoparticles in two separate steps: a rather rapid process (oxide tip growth, reduction, and sulfidization of the oxide surface) and a second step (the reduction process of the oxide core and the sulfidization of the core). This point suggests that the sulfide growth occurs from *outside in*.[22] Recently, a general rolling mechanism of layered sheets for tubule formation is proposed for the synthesis of WS_2 nanotubes on the basis of inorganic-surfactant lamellar composite.[44] Our experimental results reveal that an *inside out* mechanism postulated by Whitby et al.[41] is taking the role for the growth of WS_2 nanotubes starting from $(NH_4)_2WS_4$. The *inside out* mechanism means that first a single-wall WS_2 nanotube is formed (Figure 8), which serves as a kind of template for the following WS_2 layers, which grow on top of the first one. The schematic diagram of Figure 14 shows a possible pathway. First, the catalyst thiophene diffused into aggregations of $(NH_4)_2WS_4$, and the input energy provided by the sintering lets the atoms arrange themselves in layered structures (Figure 15a). Second, the layers curl at the edge (Figure 15b). Third, during the escaping of NH_3 and H_2S (equation 1), the layered structures rolled into tubes, leading to further growth of (single-wall, normally multiwall) nanotubes (Figure 15c). Our results indicate that the formation of WS_2 nanotubes undergoes an induction period at the initial annealing stage, which may be caused by the nucleation and growth of the WS_2 phase due to the catalysis of thiophene. Thus, the kinetics of the present gas−solid reaction is greatly improved through the ball-milling treatment. The nanotube conversion shows that the reaction rate is initially controlled by the dimensional

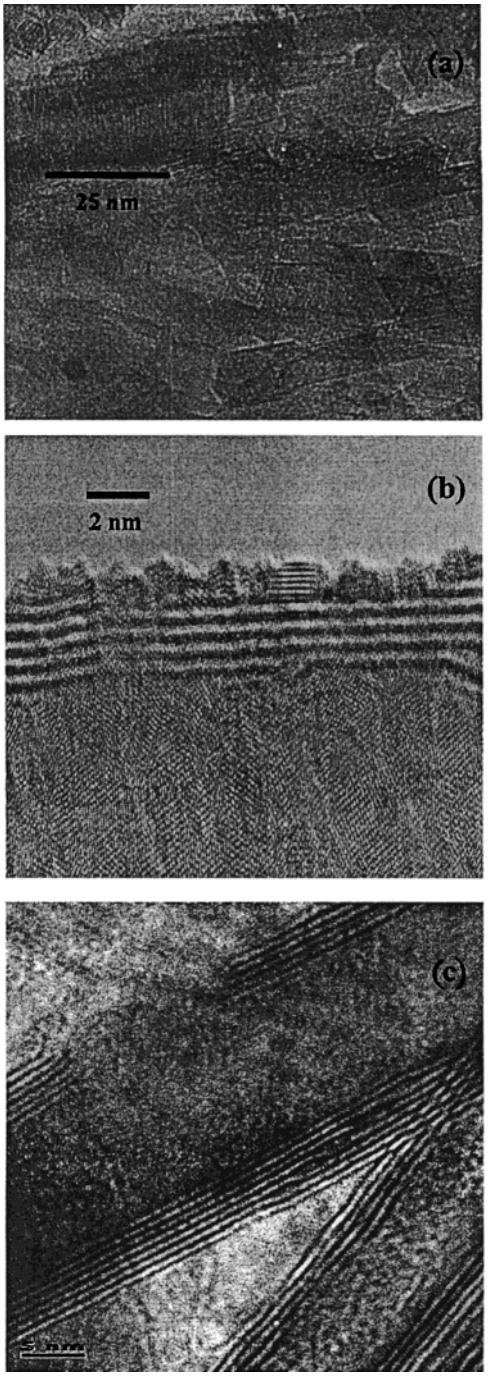

Figure 15. HRTEM images for (a) layered W−S structures, (b) the curling edge of W−S layers, (c) the formation of (single-wall and multiwall) WS_2 nanotubes.

(47) Srolovitz, D. J.; Safran, S. A.; Homyonfer, M.; Tenne, R. *Phys. Rev. Lett.* **1995**, *74*, 1779.
(48) Seifert, G.; Terrones, H.; Terrones, M.; Jungnickel, G.; Frauenheim, T. *Phys. Rev. Lett.* **2000**, *85*, 146.
(49) Moulder, J. F.; Stickle, W. F.; Sobol, P. E.; Bomben, K. D. In *Handbook of X-ray Photoelectron Spectroscopy*; Chastain, J., Ed.; Perkin-Elmer Corporation: Wellesley, MA, 1992.
(50) Gregg, S. J.; Sing, K. S. W. *Adsorption, Surface Area and Porosity*; Academic Press: San Diego, CA, 1997.
(51) Rothschild, A.; Sloan, J.; Tenne, R. *J. Am. Chem. Soc.* **2000**, *122*, 5169.

nucleation and growth, and as the formation of the WS_2 phase proceeds, a diffusion-controlled reaction gains in importance. Therefore, the present *inside out* mechanism is a very important advance in the synthesis of metal-sulfide nanotubes because the method presented here is mild and offers a path to high-purity, large-scale, and easy-control fabrication of single wall and multiwall nanotubes.

4. Conclusions

We have demonstrated a simple method to prepare high-rate and high-quality WS_2 nanotubes by ball milling $(NH_4)_2WS_4$ to obtain amorphous/nano particles with high specific surface area and loading them in a controlled thermal decomposition environment with thiophene catalyst. This technique has the capability to fabricate WS_2 nanotubes with controlled alignment at relatively low temperatures. The yield and quality of WS_2 nanotubes was greatly influenced by the synthesis parameters. The growth mechanism of obtaining WS_2 nanotubes is believed to be controlled by an *inside out* process. An important implication of our results is the possibility of large-scale and low-cost synthesis of WS_2 nanotubes, which would certainly be a great step toward exploring other layered metal-sulfide nanotubes.

Acknowledgment. We acknowledge the Scientific Research Foundation for the Returned Overseas Chinese Scholars (State Education Ministry).

CM020471F